A Multidirectional Photodiode Array for the Measurement of Solar Radiances

by

J.M. Davis, C. Vogel, and S.K. Cox

Department of Atmospheric Science
Colorado State University
Fort Collins, Colorado

Colorado State University

Department of Atmospheric Science

Paper No. 322

A MULTIDIRECTIONAL PHOTODIODE ARRAY FOR
THE MEASUREMENT OF SOLAR RADIANCES

by

J. M. Davis, C. Vogel and S. K. Cox

Department of Atmospheric Science
Colorado State University
Fort Collins, Colorado

February, 1980

Atmospheric Science Paper Number 322

A MULTIDIRECTIONAL PHOTODIODE ARRAY FOR
THE MEASUREMENT OF SOLAR RADIANCE

by

J. M. Davis, C. Vogel and S. K. Cox

Department of Atmospheric Science
Colorado State University
Fort Collins, Colorado

February, 1980

J. M. Davis, C. Vogel and S. K. Cox

ACKNOWLEDGEMENTS

TABLE OF CONTENTS

LIST OF TABLES

iv

LIST OF TABLES (Continued)

v

LIST OF FIGURES

I. INTRODUCTION

One of the primary goals of field experimentation in atmospheric radiation has been the measurement of radiative fluxes in order to provide the resulting diabatic term required in dynamic modelling. The satellite provides an ideal platform for measuring the reflected component of the net flux at the top of the earth-atmosphere system. However, due to the sampling limitations imposed by flat plate radiometers, determination of reflected fluxes on a regional scale may be best accomplished by using a scanning radiometer in conjunction with a bidirectional reflectance model to infer the upwelling flux. It has been observed that many commonly occurring reflectance patterns are highly anisotropic; see for example: Brennan and Bandeen (1970), Ruff et al. (1968) and Salomonson (1968). These observations have been carried out for specific targets (stratus clouds, ocean, desert, etc.) and, therefore, it is difficult to apply the resulting models to more generalized atmospheric scenes such as broken cloud over ocean, desert under a dust aerosol, towering cumulus over stratocumulus etc. In view of the above, further efforts in bidirectional reflectance modelling are highly desirable.

With the same goals in mind, modellers of radiative transfer in the atmosphere have developed techniques for estimating reflected flux in more realistic atmospheres including the effects of aerosols, finite clouds and clouds with a non-homogeneous microstructure. However, little experimental evidence exists which could test the validity of the various efforts. Of all the radiative properties which could be used to verify the model, one of the most difficult and thus, one which would provide the best information is the angular distribution of the radiance field within the cloud.

Scanning radiometers aboard aircraft have been used in previous efforts to obtain this type of experimental evidence. Although there are certain advantages in using the scanning radiometer, rather complicated flight patterns are required to sample the radiance field. These patterns take a rather large distance and long time interval to accomplish. This requirement is a hindrance in observing reflected fluxes over fairly large areas but may prohibit in-cloud observations altogether (especially in attempting to confirm angular radiance patterns in finite clouds).

This report describes an instrument designed to circumvent the sampling problem imposed by the scanning radiometer. It

has been developed by the Department of Atmospheric Science at
Colorado State University. It has been dubbed "the bugeye
detector" based on its visual appearance. The initial
testing of the instruments' performance took place in the
summer MONEX (Monsoon Experiment) during which two instru-
ments were mounted (one downward and one upward looking) on
NASA's Convair 990 research aircraft. Included in the report
are descriptions of the physical and electrical characteristics
of the instruments, a discussion of the mathematical methods
used in analyzing the data, comments on the initial performance
of the instruments and suggestions for future design options
based on the initial testing.

II. INSTRUMENT CHARACTERISTICS

A. Physical Characteristics

The bugeye instrument consists of an hemispherical array of thirteen silicon photodiodes and associated electrical circuitry mounted in an aluminum housing. Figure 1 gives the overall dimensions of the instrument and Table 1 gives the angular positions and the fields of view of the detectors for both configurations. The instruments will be referred to as upward looking and downward looking according to their placement on an aircraft. As indicated in Table 1, the primary differences between the two instruments are the positions of the individual detectors and their full angle fields of view.

The different fields of view of the detectors required some minor differences in the electrical circuitry of the instruments which will be described in the next section. The configurations shown in Table 1 were "first guess" selections based on the radiance field to be viewed by each instrument and the nature of the data product desired. Improvements to the initial configurations are discussed in the section on data retrieval. The 180° field of view on the upward looking detectors was provided by placing a 1 mm thick by 1 cm diameter teflon disk atop each photodiode. The cosine response curve of
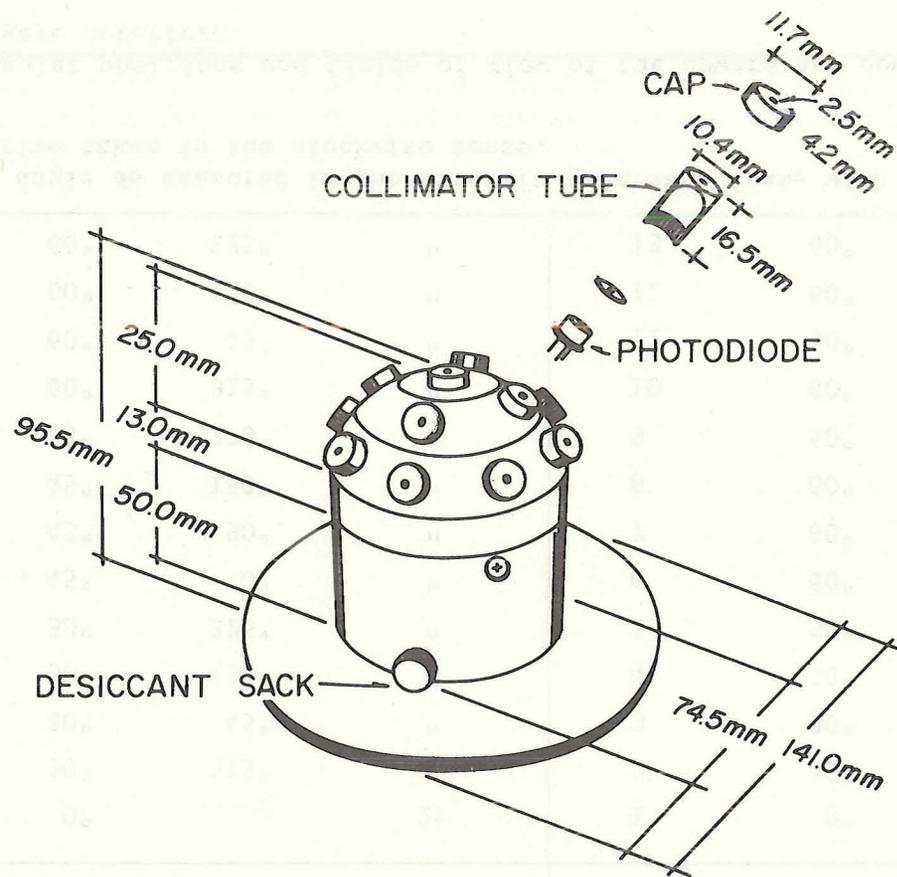
Figure 1. Dimensions of the downward looking bugeye. Overall dimensions of the upward looking bugeye are identical except for absence of the collimator tube.

UPWARD LOOKING BUGEYE				DOWNWARD LOOKING BUGEYE			
Detector Number	Angle from Zenith	Azimuth Angle *	Field of View Steradian	Detector Number	Angle from Nadir	Azimuth Angle *	Field of View Steradian
1	0°	——	2π	1	0°	——	.0239
2	30°	315°	"	2	30°	30°	"
3	30°	45°	"	3	30°	90°	"
4	30°	135°	"	4	30°	180°	"
5	30°	225°	"	5	30°	270°	"
6	45°	0°	"	6	60°	0°	"
7	45°	90°	"	7	60°	45°	"
8	45°	180°	"	8	60°	90°	"
9	45°	270°	"	9	60°	135°	"
10	60°	315°	"	10	60°	180°	"
11	60°	45°	"	11	60°	225°	"
12	60°	135°	"	12	60°	270°	"
13	60°	225°	"	13	60°	315°	"

*The azimuth angle as measured in the aircraft reference frame with the forward direction at 0° and positive taken in the clockwise sense.

Table 1. Angular positions and fields of view of the upward and downward looking bugeye detectors.

the disk is shown in Figure 2. The field of view of each detector on the downward looking instrument was limited to 10° by inserting each photodiode into the base of a collimator tube. The details of the collimator device are shown in the inset of Figure 1. The field of view of each of the thirteen detectors on the bottom instrument was nominally 10° or .0239 steradians.

The cylindrical midsection of the housing is separable from the base plate and from the diode array to allow access to the diodes and the circuit boards which are housed within. Also shown in Figure 1 is a knurled knob near the base of the bugeye. A cloth sack filled with desiccant was attached to the interior end of the knob to protect the electrical circuitry from condensation. The silicon photodiodes were mounted in sockets which were press-fitted into the aluminum housing. All other electrical components were mounted on two circular printed-circuit boards spaced about 1" apart within the cylindrical housing. All external electrical connections were made via a nineteen pin connector mounted in the center of the base plate.

B. Optical and Electrical Characteristics

Other than the field of view of the individual detectors which was discussed previously, the basic optical characteristics

Figure 2. Cosine response of the teflon-disk photodiode combination used on the upward looking bugeye.

of the instrument are those of the photodiode. The particular

diode used in the initial bugeye configuration was type SGD-100A

manufactured by EG&G, Inc. The optical characteristics of the

diode are presented in Table 2 and are quoted directly from the

manufacturer's specification sheet. The spectral response is

shown in Figure 3.

The photodiodes are operated in the photo conductive mode

in order to utilize the wide range linear response of the diode.

The output current of the device is between 0 and 1 milliampere.

This output current was converted to a 0 - 10 volt signal by

using a simple operational amplifier (Op-Amp) circuit shown in

Figure 4. By using a quad configured Op-Amp chip it was possi-

ble to enclose sixteen amplifier devices within the bugeye

housing although only thirteen of these were used. The output

voltage was scaled to the 0 - 10V range by properly selecting

the value of R_f. It is noted in Figure 4 that the dualanode of

the diode is negatively biased and this connection is made

through the diode can. As a result it was necessary to elec-

trically isolate the diode can from the bugeye housing which

allowed the bugeye housing to be maintained at the potential of

the aircraft frame. Phenolic insulators were used for this

purpose. The electrical connection to the bugeye was supplied

through a Cannon nineteen pin connector.

CHARACTERISTIC	MINIMUM	TYPICAL	MAXIMUM	UNITS AND CONDITIONS
Spectral Range	0.35		1.13	Micrometers
Spectral Sensitivity	0.45	0.5	0.65	Amps/Watt at 0.9 μm
Integrated Sensitivity				
2870°K Black Body		0.12		Amps/Watt
6000°K Black Body		0.20		Amps/Watt
Luminous Sensitivity				
2870°K Black Body		5000		μA/Lumen
6000°K Black Body		1500		μA/Lumen
Operating Voltage	0	100	180	Volts
Breakdown Voltage	200	600		Volts at 100 μA
Linearity of Response		5		% Over 7 Decades
Operating Temperature	-65	25	+150	°C
Rise Time		4×10^{-9}		Seconds at 100V
Dark Current		3×10^{-9}	20×10^{-9}	Amps at 10V at 25°C
Dark Current		10×10^{-9}	100×10^{-9}	Amps at 100V at 25°C
Capacitance		4.0	7.0	Picofarads at 100V
NEP (0.9 μm, 10^3, 1)		1×10^{-13}		Watts at 25°C
D * (0.9 μm, 10^3, 1)		2.3×10^{12}		Watts^{-1}cm Hz$^{1/2}$ at 25°C
Channel Impedance		3×10^6		Ohms at 100V at 25°C
Field of View		160		Degrees-Full Angle
D.C. Photocurrent			1.0	mA at 150V
Pulsed Photocurrent			120	mA at 150V
Power Dissipation				
D.C.			0.2	Watts
Pulsed			25	Watts (1 μ sec Max.)

Table 2. Optical and electrical characteristics of the SGD-100A photodiode.
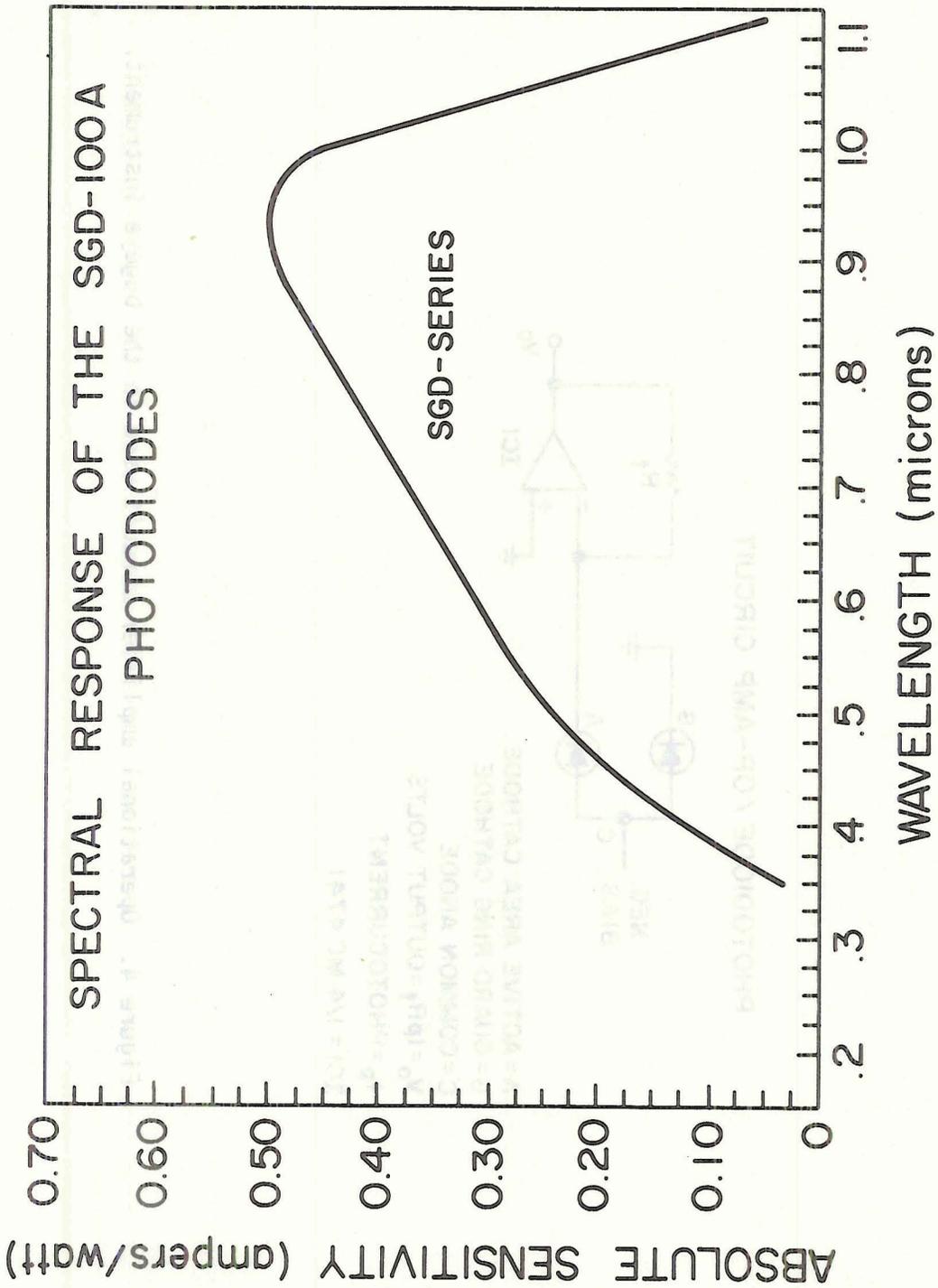
Figure 3. Spectral response of the SGD-100A photodiode.
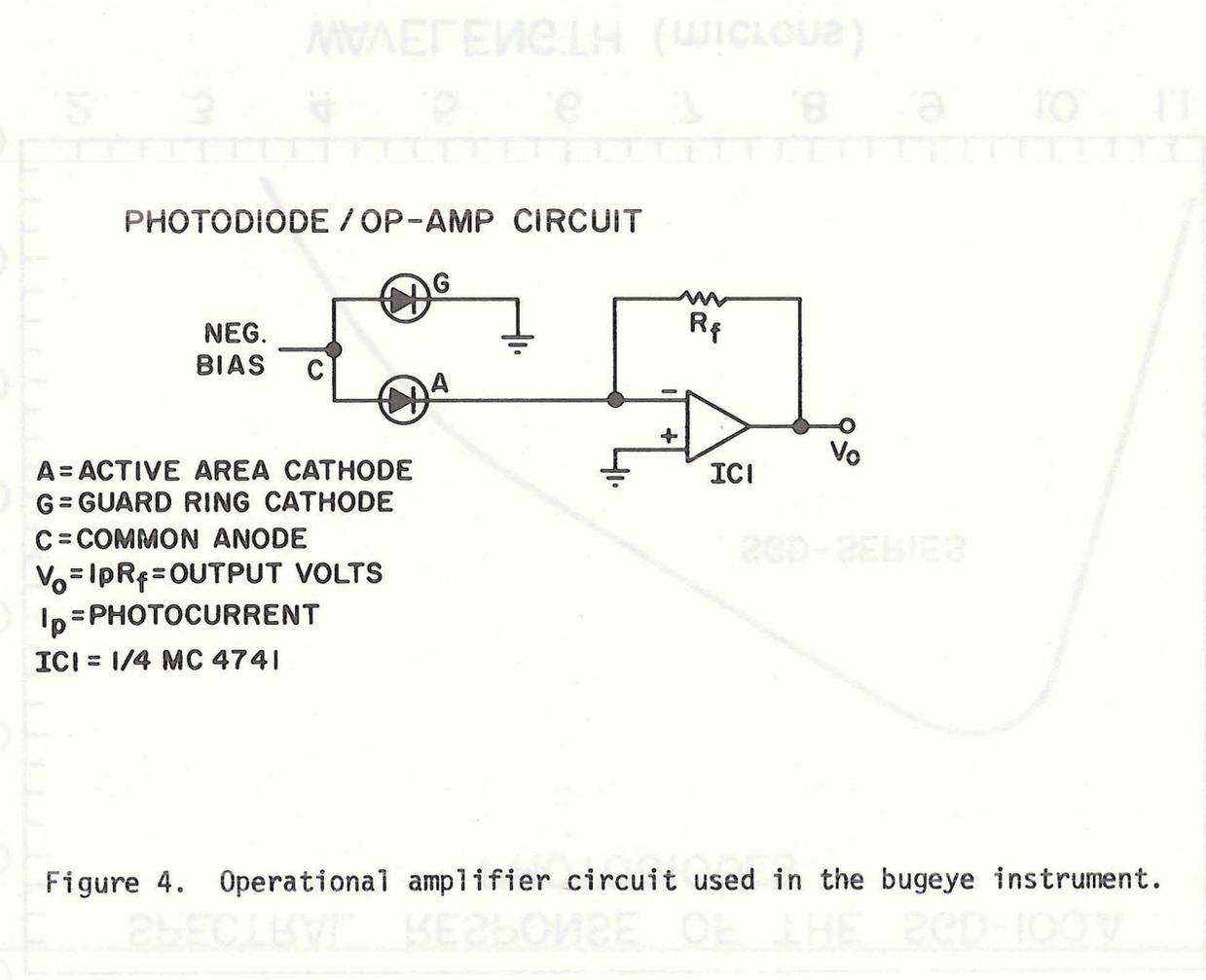
PHOTODIODE / OP-AMP CIRCUIT

NEG.
BIAS
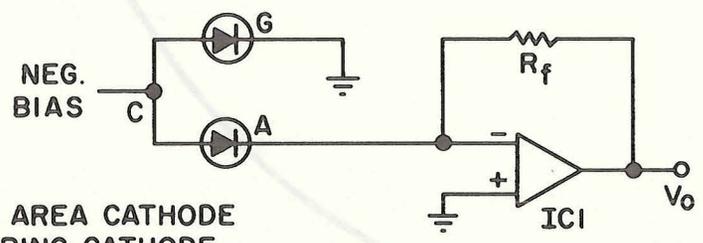
A = ACTIVE AREA CATHODE
G = GUARD RING CATHODE
C = COMMON ANODE
$V_o = I_p R_f =$ OUTPUT VOLTS
$I_p =$ PHOTOCURRENT
IC1 = 1/4 MC 4741

Figure 4.   Operational amplifier circuit used in the bugeye instrument.

C. Calibration

The utilization of a multidetector instrument provides con-
tinuous information about the angular variability of the radi-
ance field provided the relative sensitivity of each detector
is known. The difficulty of monitoring relative sensitivities
is an important consideration when deciding upon the number of
detectors which should be used. In the present case establish-
ing adequate field calibration procedures was difficult. A
portable calibration source was constructed which consisted of
a small incandescent lamp powered by dry cell batteries housed
behind a diffusing surface. A coupling attachment was mounted
at the end of the calibrator so that the device could be fitted
over each of the protruding collimator tubes of the downward
looking bugeye. In this way the position of the calibrator
(and its diffusing surface) relative to each detector was rea-
sonably constant. To reduce source variability a voltage re-
gulating circuit was employed. Also, the source was monitored
within the calibrator by a diode configured identically to
those within the bugeye. A calibration of the downward looking
instrument was performed on ten occasions prior to, during and
after the field experiment. The relative sensitivities of the
detectors varied by 5% from their mean values according to the
calibration data.

Associated with the diode and its amplifier is a noise
current consisting of Johnson noise and shot noise. These
currents are temperature dependent and generally increase with
temperature. Also, the individual amplifier gains are tempera-
ture dependent. During one flight the diodes of the downward
looking bugeye were shielded from incoming radiation. The data
from this flight indicated that the temperature dependencies of
the noise currents and the amplifier gains are nearly compensa-
tory, the voltage output in fact, increased slightly as the
temperature decreased from 25°C to -45°C. These results in-
dicate that for small temperature excursions the resulting
"dark current" offset voltage (V_{DC}) may be removed from the
signal (V_S) to yield a voltage (V_E) which is proportional to
incident irradiance (E) according to the equation

$$V_E = V_S - V_{DC} \tag{1}$$

$$= k\ E,$$

the value of k for a given detector being temperature dependent.
Since the bugeye is intended to give the relative angular
characteristics of the target radiance field (the true magnitude

being provided by a scaling of the integrated radiance pattern
to the irradiance of the target as measured by the hemispheric
radiometer), we only require that k vary with temperature in
the same manner for each detector. This behavior has not yet
been verified but is a reasonable assumption based on the
nearly identical performance of all the diode circuits during
the "shielded" flight mentioned above.

The relative values of k in Eq. (1) for each detector may
be obtained from the results of the calibration described above.
Yet to be specified, however, is the absolute magnitude of k
needed to convert the voltage values to irradiance. This con-
stant is determined by expressing the voltage in a continuous
functional form (described in the next section) and integrating
the component normal to a horizontal surface over the hemisphere
viewed by the bugeye. The resulting "voltage irradiance" is
proportional to the irradiance on the same horizontal surface
and the value of k may be found by division of the "voltage
irradiance" by the irradiance measured with a flat plate
radiometer.

III. DATA ANALYSIS

As mentioned in the previous section, the detectors provide a voltage V_i proportional to the incident irradiance E; in the spectral bandpass of the diode.

Consider an infinitesimally small region $d\omega$ in the field of view of one of the detectors of the bugeye. Let $\underset{\sim}{N}$ denote the unit vector normal to the plane of the detector, and let $\underset{\sim}{P}$ denote the position of the region $d\omega$, as shown in Figure 5.

Let $R(\underset{\sim}{P})$ denote the intensity of the radiance field at $\underset{\sim}{P}$ and let β be the angle between the unit normal vector $\underset{\sim}{N}$ and the unit vector $\underset{\sim}{P}$. Then the contribution to the irradiance measured by the detector due to $d\omega$ is given by

$$dE \;=\; \cos\beta\; R(\underset{\sim}{P})\, d\omega \;=\; (\underset{\sim}{P}\cdot\underset{\sim}{N})\, R(\underset{\sim}{P})\, d\omega. \qquad (2)$$

Integration over $\Omega(\underset{\sim}{N})$, the region viewed by the detector, yields the expression

$$E(\underset{\sim}{N}) \;=\; \int_{\Omega(\underset{\sim}{N})} (\underset{\sim}{P}\cdot\underset{\sim}{N})\, R(\underset{\sim}{P})\, d\omega, \qquad (3)$$

for the total irradiance incident upon the detector.
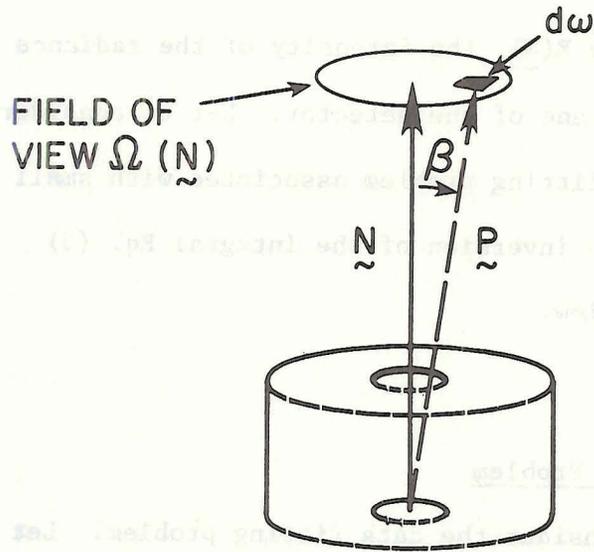
Figure 5. Geometry of the radiance field as seen by the detector.

Notice that as one restricts the field of view about the normal $\underset{\sim}{N}$, the angle β becomes small and the quantity $(\underset{\sim}{P} \cdot \underset{\sim}{N})$ approaches unity so that

$$E(\underset{\sim}{N}) \approx R(\underset{\sim}{N}) \int_{\Omega\,(N)} d\omega. \qquad (4)$$

That is, for small fields of view the measured irradiance $E(\underset{\sim}{N})$ is proportional to the $R(\underset{\sim}{N})$, the intensity of the radiance field normal to the plane of the detector. Let us consider two cases: the data fitting problem associated with small fields of view and the inversion of the integral Eq. (3) for large fields of view.

A. Data Fitting Problem

We will first consider the data fitting problem. Let $R_i = R(\underset{\sim}{N}_i)$, $i = 1, 2, \ldots, 13$, represent measurements of the radiance at the normals to each of the thirteen detectors. Suppose that the field of view of the detector is small enough that Eq. (4) is valid. For any position $\underset{\sim}{P}$ we seek an estimate of the intensity of the radiance field at $\underset{\sim}{P}$ of the form

$$\hat{R}(\underset{\sim}{P}) = C_1 \psi_1(\underset{\sim}{P}) + C_2 \psi_2(\underset{\sim}{P}) + \ldots + C_n \psi_n(\underset{\sim}{P}) \quad (5)$$

$$= \sum_{j=1}^{n} C_j \psi_j(\underset{\sim}{P})$$

where the ψ_j's are suitable approximating functions and the C_j's are coefficients to be determined. In practice we have chosen spherical harmonics as approximating functions (see Table 3), and calculate the coefficients C_1, C_2, ..., C_n minimizing the sum of squares error

$$\sum_{i=1}^{13} [R_i - \hat{R}(N_i)]^2$$

$$(6)$$

$$= \sum_{i=1}^{13} \left[R_i - \left(C_1 \psi_1(N_i) + C_2 \psi_2(N_i) + \ldots + C_n \psi_n(N_i) \right) \right]^2.$$

Although by choosing n to be 13, one could force the sum of squares error to be zero and get agreement between $\hat{R}$ and R at the normal positions $\underset{\sim}{N_i}$, this tends to give a highly unstable, oscillatory $\hat{R}$ which is a very poor estimate of R at positions $\underset{\sim}{P}$ for which measurements were not taken. Table 3 contains an analysis of the effects of various values of n on the error

NUMBER OF SPHERICAL HARMONICS	NTH SPHERICAL HARMONIC	CONDITION NUMBER	ERROR $\text{SQRT}(\overset{13}{\underset{i=1}{\Sigma}} (R_i - \hat{R}_i)^2 / \overset{13}{\underset{i=1}{\Sigma}} R_i^2)$	POINTWISE ERROR $[R(\underset{\sim}{P}) - \hat{R}(\underset{\sim}{P}) / R(\underset{\sim}{P})]$
1	1	1.000	.226155E+00	.131605E+01
2	$\cos(z)$	8.993	.108484E-01	.425655E-01
3	$\sin(z)\ \cos(a)$	8.993	.137847E-01	.507731E-01
4	$\sin(z)\ \sin(a)$	8.993	.158322E-01	.409498E-01
5	$1.5\ \cos^2(z) - .5$	91.769	.192411E-01	.103482E+00
6	$\sin(z)\ \cos(z)\ \cos(a)$	91.769	.208006E-01	.116577E+00
7	$\sin(z)\ \cos(z)\ \sin(a)$	91.769	.228886E-01	.135278E+00
8	$\sin^2(z)\ \cos(2a)$	91.769	.238563E-01	.135278E+00
9	$\sin^2(z)\ \sin(2a)$	91.769	.252618E-01	.138224E+00
10	$\cos(z)\ (5\ \cos^2(z) - 3)$	1199.369	.263551E-01	.300908E+00
11	$(5\ \cos^2(z) - 1)\ \sin(z)\ \cos(a)$	1199.369	.274585E-01	.292146E+00

Table 3.
(Page 1 of 2)

NUMBER OF SPHERICAL HARMONICS	NTH SPHERICAL HARMONIC	CONDITION NUMBER	ERROR $$\mathrm{SQRT}\left(\sum_{i=1}^{13}(R_i-\hat{R}_i)^2 / \sum_{i=1}^{13} R_i^{\,2}\right)$$	POINTWISE ERROR $[R(\underset{\sim}{P})-\hat{R}(\underset{\sim}{P})/R(\underset{\sim}{P})]$
12	$(5\cos^2(z)-1)\sin(z)\sin(a)$	1199.369	.279254E-01	.328351E+00
13	$\sin^2(z)\cos(z)\cos(a)$	$+\infty$	.279254E-01	.313247E+00

Table 3. Stability analysis for the instrument as a function of the number of basis functions used in the data fit. The hypothetical radiance field is given by $R(z,A) = \cos(z)$ with a 5% uniformly distributed random error superimposed on the test radiance field at the angular positions of the detectors. An error analysis is also given for point P not seen by any detector where $P = (z,A) = (72°, 45°)$. The analysis is an average for 10 different random error sequences.

between $\hat{R}$ and R. For this illustration R is the cosine of the zenith angle. One should note that the error between $\hat{R}$ and R depends not only on n, but also on the radiance field R. For this reason we have included in our table the condition number (Lawson and Hanson, 1974) of the system given by Eq. (6). The condition number, which is the ratio of the largest eigenvalue to the smallest eigenvalue of a linear system, gives a measure of the stability of Eq. (6) that is independent of the radiance field R. While a large value of n yields an unstable estimate $\hat{R}$, too small a choice of n yields a very smooth estimate which may lack the variability needed to fit many radiance fields effectively. On the basis of experimentation we have found that n = 5 is usually adequate.

B. Integral Equation Inversion

Applying Eq. (3) to the estimate $\hat{R}$ of R given in Eq. (5) yields the expression

$$
\hat{E}(\underset{\sim}{N}) = \int_{\Omega(\underset{\sim}{N})} (\underset{\sim}{P} \cdot \underset{\sim}{N}) \left[\sum_{j=1}^{n} C_j \psi_j(\underset{\sim}{P}) \right] d\omega
$$

$$
= \sum_{j=1}^{n} C_j H_j(\underset{\sim}{N}),
$$

(7)

where $H_j(\underset{\sim}{N}) = \displaystyle\int_{\Omega(\underset{\sim}{N})} (\underset{\sim}{P} \cdot \underset{\sim}{N})\, \psi_j(\underset{\sim}{P})\, d\omega$. To determine the coefficients C_j one could take an approach similar to that used above with the narrow field of view detector and choose $C_1, C_2, \ldots, C_n$ to minimize the sum of squares error

$$\sum_{i=1}^{13} [E(\underset{\sim}{N}_i) - \hat{E}(\underset{\sim}{N}_i)]^2 \tag{8}$$

$$= \sum_{i=1}^{13} \left[E(\underset{\sim}{N}_i) - \left(C_1\, H_1(\underset{\sim}{N}_i) + C_2\, H_2(\underset{\sim}{N}_i) + \ldots + C_n\, H_n(\underset{\sim}{N}_i) \right) \right]^2 .$$

The stability of the system is very dependent upon the size of the field of view, as is illustrated in Table 4.

For small fields of view the system (Eq. 8) is almost equivalent to the system (Eq. 6). However, for larger fields of view, the system (Eq. 6) becomes so unstable that even by using fewer than thirteen spherical harmonics one still cannot find an adequate estimate of $\hat{R}(\underset{\sim}{P})$. In this case we turn to smoothing techniques discussed by Twomey (1977) and choose coefficients $C_1, \ldots, C_n$ to minimize the quantity

$$\sum_{i=1}^{13} [\hat{E}_1 - E(N_i)^2 + \gamma [S(\hat{R})]^2 , \tag{9}$$

HALF-ANGLE OF FIELD OF VIEW DEGREES	CONDITION NUMBER	ERROR $\text{SQRT}(\Sigma R_i - \hat{R}_i)^2 / \Sigma R_i^2)$
5.0	91.731	.193828E-01
10.0	91.399	.198712E-01
15.0	90.876	.208732E-01
20.0	90.206	.225850E-01
25.0	89.446	.251616E-01
30.0	88.671	.286969E-01
35.0	106.353	.344307E-01
40.0	144.889	.447267E-01
45.0	245.755	.713749E-01
50.0	384.993	.101896E+00

Table 4. Stability analysis for the inversion of Eq. (6) as
a function of the half angle of the field of view
of the detector. The hypothetical radiance field
is given by $R(z,A) = \cos(z)$ with a 5% uniformly
distributed random error superimposed on E_i. The
approximation $\hat{E}$ is made using five basis functions
and the values given are an average for 10
different random error sequences.

where $S(\hat{R})$ symbolizes some measure of the smoothness of the estimate $\hat{R}(P)$.

As the size of the field of view of a detector increases, the detector gathers more information about the radiance field. However, one must then use more sophisticated and expensive techniques to calculate an estimate of the radiance field. These considerations will be discussed later in more detail.

One example of the type of information which may be obtained from the bugeye instrument is the radiance pattern emanating from an ocean surface under clear sky conditions. The values given in Table 5 are instantaneous measurements from the bugeye. Also given are the coefficients of the spherical harmonic basis functions obtained in the manner described above, the r.m.s. error of the fit evaluated at the detector positions, the solar zenith angle and the solar azimuth. Figure 6 shows a polar plot of the (.3 to 3.0 μm) radiance field for nadir angles between 0° and 20°. A sunglint pattern is evident and is one of the most persistent patterns examined up to the present time.

C. Solution of the Direct-Diffuse Problem

One application of the bugeye instrument is for determining what fraction of incident solar radiation is direct and

Sensor (i)	Nadir Angle (z_i) of Sensor	Azimuth Angle (A_i) of Sensor	Measurement $(R_i$ of Sensor in Volts	Calculated "Radiance Voltage $(\hat{R}_i)$ at Sensor Position in Volts	ERROR $(R_i - \hat{R}_i)$
1	0°	–	.73	.71	.02
2	30°	0°	.60	.54	.06
3	30°	90°	.54	.61	-.07
4	30°	180°	.66	.67	-.01
5	30°	270°	.56	.61	-.05
6	60°	0°	.56	.53	.03
7	60°	45°	.58	.56	.02
8	60°	90°	.61	.64	-.03
9	60°	135°	.70	.73	-.03
10	60°	180°	.84	.76	.08
11	60°	225°	.73	.73	0
12	60°	270°	.67	.64	.03

Coefficient of the jth spherical harmonic C_j

$.200 \times 10^1$

-2.44×10^1

$.130 \times 10^0$

$.750 \times 10^{-1}$

$.144 \times 10^1$

r.m.s. error of fit = 0.43 volts

Table 5. Typical data and results from the instruments viewing a clear ocean sunglint pattern. Values of R_i and measured voltages, C_j represents the jth weighting of the jth spherical harmonic basis function. Also given are the r.m.s. errors of the fit at the detector positions. The solar zenith was 21.2° and the solar azimuth was 103° measured positive west of south.
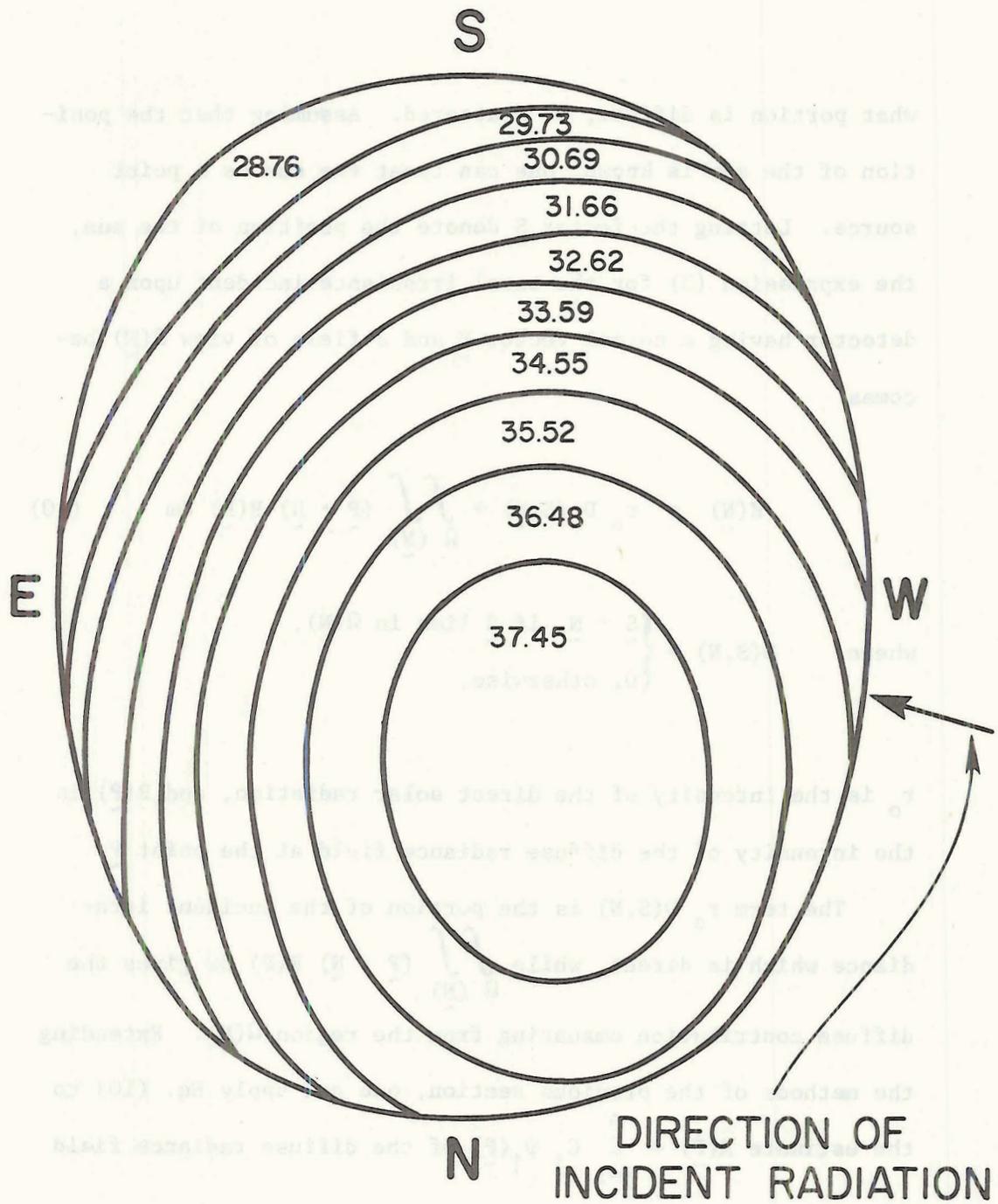
Figure 6. Polar plot of the radiance field characteristic of the sunglint. The .3 to 3 μm radiance field in watts m^{-2} sr^{-1} is shown for the nadir angle between 0° and 20°. The solar zenith angle was 21.2° and the solar azimuth was 103° measured positive west of south.

what portion is diffuse, or scattered. Assuming that the position of the sun is known, one can treat the sun as a point source. Letting the fector $\underset{\sim}{S}$ denote the position of the sun, the expression (3) for the total irradiance incident upon a detector having a normal vector $\underset{\sim}{N}$ and a field of view $\Omega(\underset{\sim}{N})$ becomes

$$E(\underset{\sim}{N}) = \dot{r}_o D(\underset{\sim}{S}, \underset{\sim}{N}) + \iint\limits_{\Omega(\underset{\sim}{N})} (\underset{\sim}{P} \cdot \underset{\sim}{N}) R(\underset{\sim}{P}) \, d\omega \qquad (10)$$

where
$$D(S,N) = \begin{cases} \underset{\sim}{S} \cdot \underset{\sim}{N}, & \text{if } \underset{\sim}{S} \text{ lies in } \Omega(\underset{\sim}{N}), \\ 0, & \text{otherwise,} \end{cases}$$

r_o is the intensity of the direct solar radiation, and $R(\underset{\sim}{P})$ is the intensity of the diffuse radiance field at the point $\underset{\sim}{P}$.

The term $r_o D(S,N)$ is the portion of the incident irradiance which is direct, while $\iint\limits_{\Omega(\underset{\sim}{N})} (\underset{\sim}{P} \cdot \underset{\sim}{N}) R(\underset{\sim}{P}) \, d\omega$ gives the diffuse contribution emanating from the region $\Omega(\underset{\sim}{N})$. Extending the methods of the previous section, one can apply Eq. (10) to the estimate $\hat{R}(\underset{\sim}{P}) = \sum\limits_{j=1}^{n} C_j \psi_j(\underset{\sim}{P})$ of the diffuse radiance field

arriving at the expression

$$\hat{E}(\underset{\sim}{N}) = \hat{r}_o D(\underset{\sim}{S}, \underset{\sim}{N}) + \sum\limits_{j=1}^{n} C_j H_j(\underset{\sim}{N}) \qquad (11)$$

where H_{ij} is defined as in Eq. (7). As before the n+1 coefficients $\hat{r}_o$, C_1, ..., C_n can be determined from the thirteen bug-eye detector measurements by minimizing the sum of squares error

$$\sum_{i=1}^{13} [E(\underset{\sim}{N_i}) - E(\underset{\sim}{N_i})]^2$$

(12)

$$= \sum_{i=1}^{13} \left[E(\underset{\sim}{N_i}) - \left(\hat{r}_o \, D \, (\underset{\sim}{S}, \underset{\sim}{N_i}) + C_1 \, H_1 \, (\underset{\sim}{N_i}) + \ldots + C_n \, H_n \, (\underset{\sim}{N_i}) \right) \right]^2 .$$

Assuming that the coefficients minimizing Eq. (12) can be found, $\hat{r}_o$ gives an estimate of the direct solar intensity $\hat{r}_o$. Table 6 gives an example of solving the direct-diffuse problem with simulated data in which the direct and diffuse components remain constant, but the solar zenith angle is allowed to vary. In Figure 7 the percentage error in the direct component is plotted against α, the ratio of the direct to the total irradiance. Figure 7 shows that whenever the direct component is greater than or equal to 2/10 of the total irradiance the percent error in the inferred direct component is less than 5% for solar zenith angles between 0° and 60°.

Solar Zenith Angle	Condition Number	Error $\text{SQRT}[\Sigma(R_i - \hat{R}_i)^2 / \Sigma R_i^2]$	Error $|r_o - \hat{r}_o| / r_o$
0.0°	.178031E+03	.233565E-01	.296561E-01
10.0°	.169719E+03	.238908E+00	.272912E-01
20.0°	.164134E+03	.237571E+00	.285568E-01
30.0°	.105385E+03	.244924E-01	.299244E-01
40.0°	.132697E+03	.474049E-01	.161799E-01
50.0°	.132275E+03	.475473E-01	.154594E-01
60.0°	.997529E+02	.257364E-01	.272666E-01
70.0°	.985964E+02	.257364E-01	.273032E-01

Half-angle of field of view for each bugeye detector = 25.0 degrees

Table 6. Stability and error analysis for the direct-diffuse problem as a function of solar zenith angle, using thirteen detectors with identical fields of view.
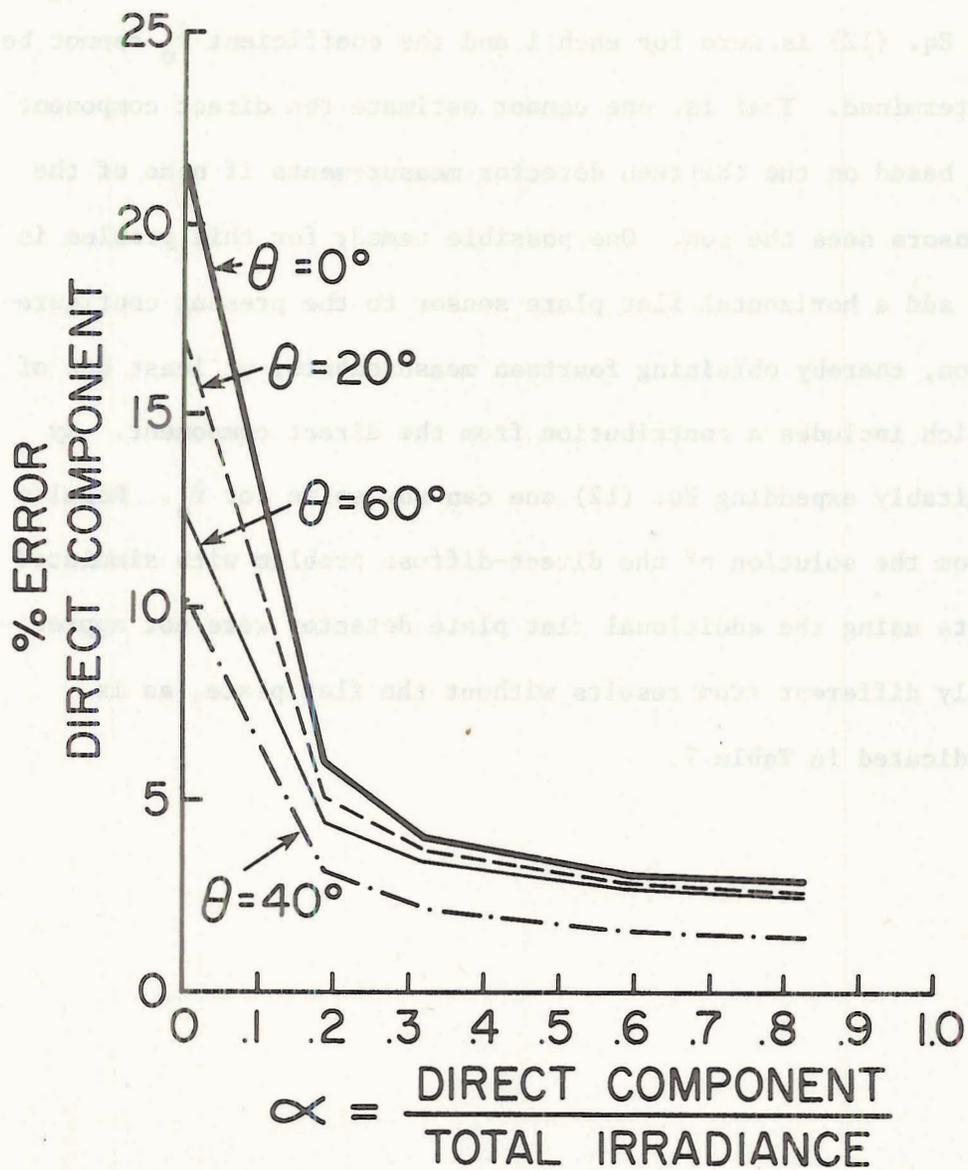
Figure 7. Error in the inferred direct component as a
function of the ratio of the direct to total
irradiance.

D. Using a Flat-Plate Detector in Conjunction with the

Multidirectional Array

Note that if none of the thirteen bugeye detectors have
the sun in their respective fields of view, the term $D(\underset{\sim}{S},\underset{\sim}{N}_i)$
in Eq. (12) is zero for each i and the coefficient $\hat{r}_o$ cannot be
determined. That is, one cannot estimate the direct component
r_o based on the thirteen detector measurements if none of the
sensors sees the sun. One possible remedy for this problem is
to add a horizontal flat plate sensor to the present configura-
tion, thereby obtaining fourteen measurements, at least one of
which includes a contribution from the direct component. By
suitably expanding Eq. (12) one can now solve for $\hat{r}_o$. Results
from the solution of the direct-diffuse problem with simulated
data using the additional flat plate detector were not appreci-
ably different from results without the flat plate, as is
indicated in Table 7.

SOLAR ZENITH ANGLE	CONDITION NUMBER	ERROR $SQRT[\Sigma(R_i - \hat{R}_i)^2 / \Sigma R_i]$	ERROR $|r_o - \hat{r}_o| / r_o$
0.0°	.319127E+03	.572601E-01	.265079E-01
10.0°	.246543E+03	.252097E+00	.276363E-01
20.0°	.235853E+03	.249850E+00	.288681E-01
30.0°	.184591E+03	.620064E-01	.262519E-01
40.0°	.189885E+03	.863504E-01	.165247E-01
50.0°	.184138E+03	.814660E-01	.166120E-01
60.0°	.170769E+03	.578737E-01	.260455E-01
70.0°	.165733E+03	.480275E-01	.276731E-01

Half-angle of field of view for each bugeye detector = 25.0 degrees

Table 7. Stability and error analysis for the direct-diffuse problem as a function of solar zenith angle using thirteen detectors with equal fields of view plus a detector with a 2π steradian field of view.

IV. INITIAL PERFORMANCE

The upward and downward looking bugeye instruments
were installed on NASA's Convair 990 research aircraft
in May, 1979 and were flown on approximately 30 missions
for a total of over 150 flight hours. Except for an
initial problem with the bottom seal of the downward looking
bugeye and an apparent instability in the upward looking bug-
eye's amplifier circuitry, both instruments performed as ex-
pected. The instability in the upward looking instrument was
not detected until about midway through the experiment. At
that time it was observed that if the instrument's orientation
with respect to the sun was such that one of the four channels
of a particular quad Op-Amp circuit was driven to a relatively
high level while another channel of the same quad amplifier was
being driven at a relatively low level, the low level output
voltage would swing negative.

Apart from the problems discussed above both instruments
performed well. The outputs from both instruments were re-
markably noise free at the resolution level of the data acqui-
sition system. The downward looking bugeye responded well to
the upwelling radiance features. For example, it was visually
confirmed that the passage of underlying clouds, lakes, rivers

and the persistent sunglint feature were detected by various
channels of the bugeye. The peak output voltages of the upward
locking instrument were well below the 10 volt upper limit of
the data system; typically remaining below 7 volts. The peak
voltage observed from the downward instrument slightly exceeded
the 10 volt limit on occasion when flying over or through the
tops of thick cirrus clouds. On these occasions the downward
looking Eppley (.3 to 3 μm) pyranometer measured an upward
irradiance greater than 1000 watts m^{-2}. Both instruments per-
formed with a high degree of consistency throughout the experi-
ment.

As an example of the instrument's initial performance
Figure 8 is presented, which shows values of reflected short-
wave flux measured over variable undercast conditions during
one of the missions in MONEX. Shown in the figure are values
of upwelling flux measured by an Eppley (.3 to 3 μm) pyrano-
meter and the corresponding values obtained from integrating
the fitted radiance field from the downward looking bugeye.
A constant proportionality factor was used to scale the bugeye
irradiance to that of the pyranometer. As indicated in the
figure agreement between the two instruments is best at the
higher values and worst at the lower values. Although choosing
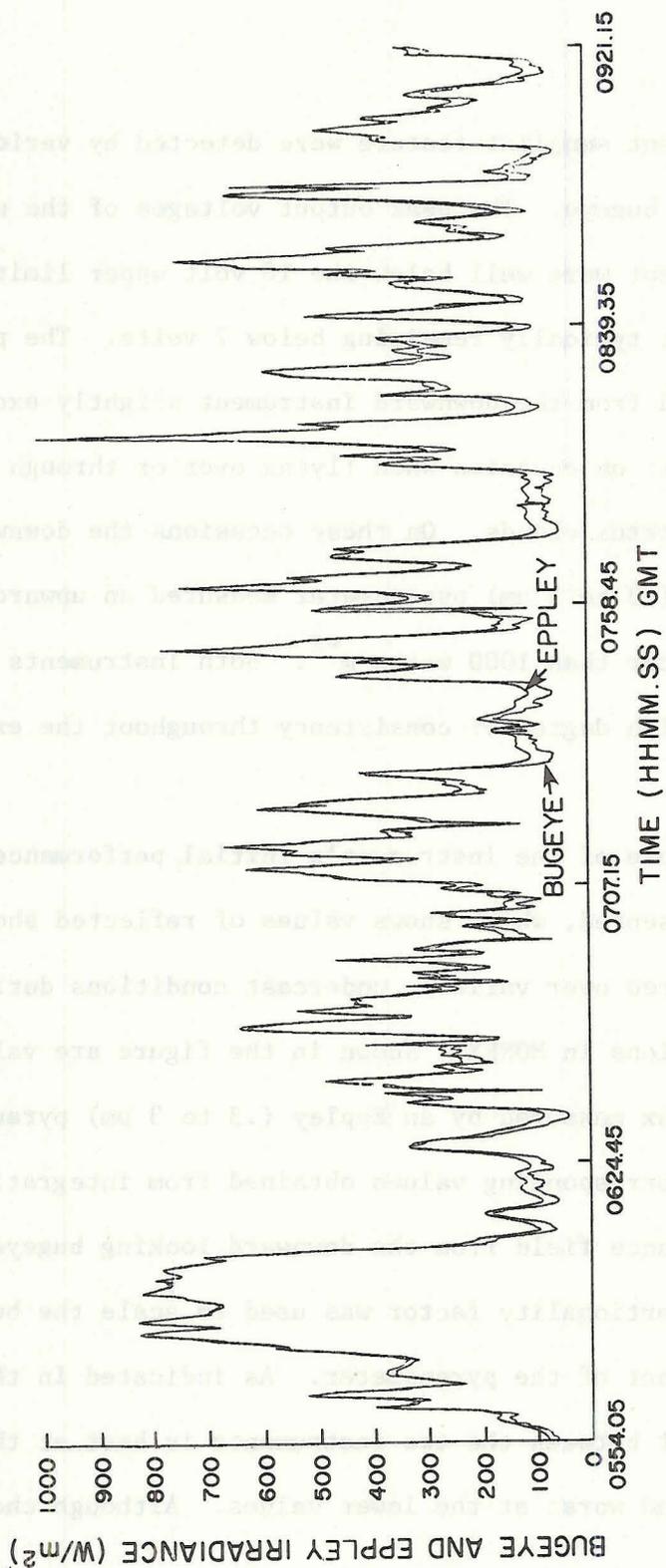
Figure 8. Comparison of the reflected solar irradiance measured by an Eppley solar (.3 – 3.0 μm) pyranometer to the integrated bugeye measurements.

a different constant of proportionality would have resulted
in a more even dispersion of the differences throughout the
range of irradiance values, additional results indicate that
the choice displayed in the figure is optimal. The additional
data (not presented here) indicate that the downward looking
bugeye's limited view of the horizon is responsible for an
underestimate of the upwelling flux when all detectors see the
relatively dark sea surface and none of the detectors view the
relatively bright horizon. Thus, for the high values dis-
played in Figure 8, which were taken in or above thick cirrus
clouds, all detectors view the cloud. Since there is little if
any separation between the cloud and the aircraft the entire
field of view of the pyranometer is also likely to be filled
by the cloud. As the aircraft exits the region of high cloud
and enters one of scattered low cloud or clear ocean conditions,
the relatively bright cloud is lost from the bugeye field of
view when it is beyond 65° from the nadir. The flat plate
radiometer continues to receive a contribution from the cloud
just exited and from other clouds above 65° from the nadir.
The next section describes a configuration of the instrument
which will improve upon the bugeye's ability to resolve the
radiance field near the horizon.

V. FUTURE DESIGN OPTIONS

It was indicated above that the physical and electrical performances of the bugeye were satisfactory except for the apparent instability in the circuitry of the upward looking instrument. Thus the suggestions for improvement pertain to the optical characteristics of the bugeye.

If the goal of the experiment is to acquire data relevant to the angular variability of the incident or reflecged short-wave radiance field, the spectral response of the sensor should be uniform across the .3 to 3 μm region of the solar spectrum. It is obvious from Figure 3 that the photodiode presently employed does not meet this requirement. Since solid state devices in general cannot respond in the required manner, perhaps the next best solution is to utilize a photodiode with uniform spectral response in the visible wavelength.

As mentioned previously, calibration of a multidetector instrument is not a simple matter due to the possibility of variation in source intensity while moving the calibrator from detector to detector and inconsistencies in positioning the calibration device with respect to the detectors. An ideal solution would be construction of an integrating sphere which could be used to calibrate all of the detectors simultaneously

and whose orientation with respect to the entire instrument
could be more surely fixed.

It was pointed out previously that the choice of the size
of the field of view of the detectors depends on two conflicting
considerations. The smaller the field of view, the easier it
is to estimate the radiance field based on detector measure-
ments. On the other hand, the larger the field of view, the
more information one gathers about the radiance field. To
accommodate both considerations, one must in some sense "spread"
the detectors evenly about the hemisphere to reduce the amount
that different fields of view overlap. Based upon the results
shown in Table 7 where the condition number does not deteriorate
substantially until the field of view exceeds 60°, and the re-
quirements that we sample as much of a 2π steradian field with
thirteen detectors as possible while still minimizing sensor
view overlap, we have selected a 50° field of view arranged in
the manner shown in Table 8. This configuration yields satis-
factory results for simulated radiance fields and should be
adequate for many applications.

MODIFIED SENSOR CONFIGURATION FOR BUGEYE

SENSOR NUMBER	ANGLE FROM ZENITH	AZIMUTH ANGLE
1	0.0°	–
2	30.0°	0.0
3	30.0°	120.0
4	30.0°	240.0
5	45.0°	60.0
6	45.0°	180.0
7	45.0°	300.0
8	60.0°	30.0
9	60.0°	90.0
10	60.0°	150.0
11	60.0°	210.0
12	60.0°	270.0
13	60.0°	330.0

Table 8. Proposed positioning of the detectors in order to maximize information content collected by bugeye.

VI. CONCLUSIONS

An instrument designed to measure the angular variation of a radiance field in the .3 to 1.1 μm spectral bandpass is described. The instrument consists of thirteen photodiode detectors mounted in fixed positions. Data analysis procedures designed to produce a continuous depiction of the radiance field over a 2π steradian solid angle from the thirteen discrete observations are described. These analysis procedures utilize spherical harmonics basis functions as a means of interpolation between the thirteen discrete radiance observations. An analysis procedure used to infer the direct component of the solar irradiance is also given.

A modified sensor configuration selected upon the basis of satisfying the analytical procedures, sampling a 2π steradian field of view and minimizing sensor overlap is given.

REFERENCES

Brennan, B., and W. R. Bandeen, 1970: Anisotropic reflectance characteristics of natural earth surfaces. J. Appl. Opt., 9, 405-412.

Lawson, Charles L., and Richard J. Hanson, 1974: Solving Least Squares Problems. Prentice-Hall, Inc.

Ruff, I., R. Koffler, S. Fritz, J. S. Winston, and P. K. Rao, 1968: Angular distribution of solar radiation reflected from clouds as determined from TIROS-IV radiometer measurements. J. Atmos. Sci., 25, 323-332.

Salomonson, V. V., 1968: Anisotropy in reflected solar radiation. Atmos. Sci. Pap. 128, Colorado State University, 143 pp.

Twomey, S., 1977: Introduction to the Mathematics of Inversion in Remote Sensing and Indirect Measurements. Elsevier Scientific Publishing Company.

BIBLIOGRAPHIC DATA SHEET	1. Report No. CSU-ATS- 322	2.	3. Recipient's Accession No.
4. Title and Subtitle A MULTIDIRECTIONAL PHOTODIODE ARRAY FOR THE MEASUREMENT OF SOLAR RADIANCES			5. Report Date February, 1980
			6.
7. Author(s) S. K. Cox, J. M. Davis and C. Vogel			8. Performing Organization Rept. No. CSU-ATS- 322
9. Performing Organization Name and Address Department of Atmospheric Science Colorado State University Fort Collins, Colorado 80523			10. Project/Task/Work Unit No.
			11. Contract/Grant No. ATM 78-12631
12. Sponsoring Organization Name and Address National Science Foundation GARP 1800 G. Street, N.W. Washington, D.C. 20550			13. Type of Report & Period Covered
			14.

15. Supplementary Notes

16. Abstracts

An instrument designed to measure the angular variation of a radiance field in the .3 to 1.1 μm spectral bandpass is described. The instrument consists of thirteen photodiode detectors mounted in fixed positions. Data analysis procedures designed to produce a continuous depiction of the radiance field over a 2π steradian solid angle from the thirteen discrete observations are described. These analysis procedures utilize spherical harmonics basis functions as a means of interpolation between the thirteen discrete radiance observations. An analysis procedure used to infer the direct component of the solar irradiance is also given.

A modified sensor configuration selected upon the basis of satisfying the analytical procedures, sampling a 2π steradian field of view and minimizing sensor overlap is given.

17. Key Words and Document Analysis. 17a. Descriptors

Radiative measurements
Bidirectional reflectance
Reflectance patterns
Radiation instrumentation

17b. Identifiers/Open-Ended Terms

17c. COSATI Field/Group

18. Availability Statement	19. Security Class (This Report) UNCLASSIFIED	21. No. of Pages 42
	20. Security Class (This Page)	22. Price